Quantitative "Hot-Spot" Imaging of Transplanted Stem Cells Using Superparamagnetic Tracers and Magnetic Particle Imaging

Jeff W.M. Bulte[1,2,3,4], Piotr Walczak[1], Miroslaw Janowski[1], Kannan M. Krishnan[5], Hamed Arami[5], Aleksi Halkola[6], Bernhard Gleich[7], and Jürgen Rahmer[7]

[1]Russell H. Morgan Department of Radiology and Radiological Science, Division of MR Research and Cellular Imaging Section, Institute for Cell Engineering, and [2]Departments of Chemical and Biomolecular Engineering, [3]Biomedical Engineering, and [4]Oncology, Johns Hopkins University School of Medicine, Baltimore, MD; [5]Departments of Materials Science and Physics, University of Washington, Seattle, WA; [6]Philips Healthcare, Vantaa, Finland; and [7]Philips GmbH Innovative Technologies, Research Laboratories, Hamburg, Germany

Corresponding Author:
Jeff W.M. Bulte, PhD
Department of Radiology, Johns Hopkins University School of Medicine, Miller Research Building Room 659, 733 N. Broadway, Baltimore, MD 21205;
E-mail: jwmbulte@mri.jhu.edu

Key Words: magnetic particle imaging, MPI, stem cells, cell tracking, superparamagnetic iron oxide, SPIO

Abbreviations: Feridex (F), magnetic particle imaging (MPI), magnetic particle spectroscopy (MPS), magnetic resonance imagining (MRI), mesenchymal stem cell (MSC), neural stem cell (NSC), optical density (OD), Resovist (R), superparamagnetic iron oxide (SPIO), transmission electron microscope (TEM), vibrating sample magnetometer (VSM)

ABSTRACT

Magnetic labeling of stem cells enables their noninvasive detection by magnetic resonance imaging (MRI). In practical terms, most MRI studies have been limited to the visualization of local engraftment because other sources of endogenous hypointense contrast complicate the interpretation of systemic (whole-body) cell distribution. In addition, MRI cell tracking is inherently nonquantitative in nature. We report herein on the potential of magnetic particle imaging (MPI) as a novel tomographic technique for noninvasive "hot-spot" imaging and quantification of stem cells using superparamagnetic iron oxide (SPIO) tracers. Neural and mesenchymal stem cells, representing small and larger cell bodies, were labeled with 3 different SPIO tracer formulations, including 2 preparations (Feridex and Resovist) that have previously been used in clinical MRI cell-tracking studies. Magnetic particle spectroscopy measurements demonstrated a linear correlation between MPI signal and iron content for both free particles in homogeneous solution and for internalized and aggregated particles in labeled cells over a wide range of concentrations. The overall MPI signal ranged from 1×10^{-3} to 3×10^{-4} Am^2/g Fe, which was equivalent to 2×10^{-14} to 1×10^{-15} Am^2 per cell, indicating that cell numbers can be quantified with MPI analogous to the use of radiotracers in nuclear medicine or fluorine tracers in ^{19}F MRI. When SPIO-labeled cells were transplanted in the mouse brain, they could be readily detected by MPI at a detection threshold of about 5×10^4 cells, with MPI/MRI overlays showing an excellent agreement between the hypointense MRI areas and MPI hot spots. The calculated tissue MPI signal ratio for 100 000 vs 50 000 implanted cells was 2.08. Hence, MPI can potentially be further developed for quantitative and easy-to-interpret, tracer-based noninvasive cell imaging, preferably with MRI as an adjunct anatomical imaging modality.

INTRODUCTION

Magnetic resonance imaging (MRI) cell tracking using superparamagnetic iron oxide (SPIO) particles has increased our understanding of cell biology and developing stem cell therapy (1). However, because of its indirect detection of cells through the SPIO effect on proton relaxation, there are several limitations that prevent its full exploitation. These include (1) the difficulty of absolutely quantifying cell concentration and iron content, part of which relies on the existence of different relaxation regimes (dependent on the agglomeration state and SPIO cluster size); (2) the difficulty of discriminating SPIO-labeled cells in areas of hemorrhage and traumatic injury (which are often present in targets of cell therapy), as caused by the proton-dephasing effects of methemoglobin, ferritin, and hemosiderin (especially at higher fields); (3) the occasional misinterpretation of isolated "black spots" resulting from differences in magnetic susceptibility effects around blood vessels and air-tissue interfaces (eg, the stomach and gastrointestinal tract); and (4) the inability to track cells in areas devoid of a proton signal (eg, the lungs). ^{19}F MRI cell tracking can overcome several of these

ISSN 2379-1381 http://dx.doi.org/10.18383/j.tom.2015.00172

limitations (2), including cell quantification and "hot-spot" tracer imaging (3) but suffers from an inherent lack of sensitivity and the limited availability of hardware (dual-tunable coils and interfaces).

In this study, we determined the feasibility of developing cellular magnetic particle imaging (MPI) as a new approach for noninvasively tracking cells. We originally introduced the concept of MPI cell tracking already in 2008 (4), 3 years after the initial publication of MPI by Gleich and Weizenecker (5). MPI technology is based on the principle that SPIO nanoparticles can be magnetized by an external magnetic field and exhibit a nonlinear response in a near-zero magnetic field. When the external field changes around the value 0, the magnetization will follow until it reaches a positive or negative saturation value for larger positive or negative magnetic fields. In the basic MPI scanner setup, a magnetic gradient field is created in such a manner that there is only 1 point in the 3D imaging volume at any given time at which the magnetic field is 0. Only at this point, the so-called "field-free point," will it be possible to observe oscillating changes in magnetization if an additional, oscillating external magnetic field is applied (typically in the kilohertz range). These changes are detected via magnetic induction in a sensing radiofrequency coil, much like in MRI.

Based on previously developed labeling protocols and assays for MRI cell tracking, we investigated the magnetic response of SPIO-labeled mesenchymal stem cells (MSCs) and neural stem cells (NSCs) with magnetic particle spectroscopy (MPS). Labeled MSCs were implanted in the mouse brain, and the sensitivity of MPI cell detection was determined and compared with conventional, simultaneous MRI experiments.

METHODOLOGY

SPIO Formulations

Two commercial formulations (Feridex, Berlex Imaging, Wayne, NJ; Resovist, Bayer-Schering, Berlin, Germany) that have been previously applied for clinical MRI cell tracking (6) and 1 experimental preparation (UW) custom-tailored as an MPI tracer were used in his study. UW particles were synthesized by thermal decomposition of iron oleate in the presence of oleic acid and 1-octadecene as described previously (7). Particles were purified using a 1:1 (v/v) mixture of chloroform and methanol and magnetic sedimentation. The final SPIO formulation was coated with polyethylene glycol (MW = 2 kDa; Laysan Bio Inc., Arab, AL) (8). Aggregated particles were removed by centrifugation at 3000 rpm. An inductively coupled plasma atomic emission spectrophotometer (Thermo Jarrell, Franklin, MA) was used to measure the final iron concentration in the sample. The iron concentration of the preparation was 1.70 mg of Fe per milliliter. Room temperature magnetization was analyzed using a vibrating sample magnetometer (VSM) (Lakeshore, Weterville, OH). The iron oxide crystal core size was calculated using Chantrell fitting to the VSM magnetization curve and by examination using a transmission electron microscope (TEM) (FEI TecnaiTM G2 F20, 200 KeV; Hillsboro, OR) analysis. We also used dynamic light scattering (Zetasizer Nano; Malvern Instruments, UK) to determine the overall particle hydrodynamic size of the polyethylene glycol-conjugated final SPIO preparation.

Cell Labeling and Sample Preparation

As NSCs, we used the immortalized mouse cell line C17.2, and rat MSCs were freshly isolated from bone marrow using standard procedures (9). Cells were labeled with Resovist and Feridex, and UW particles were combined with poly-L-lysine (24-48-h incubation at 25 μg of Fe per milliliter of culture medium) (10). We have chosen these 2 cell types to assess the MPS signal dependence on cell size and cytoplasmic iron content for smaller cells (NSCs, $\sim$10 μm) and larger cells (MSCs, $\sim$25 μm). Cells were washed and counted, and 50-μL gelatin (8% w/v) samples containing between 2.5×10^3 and 1×10^6 cells were prepared. Gelatin samples containing SPIO particles only (without cells) were included as a control.

The mean cellular iron content was determined using a ferrozine-based spectrophotometric assay (10). Briefly, 50-μL perchloric acid-digested labeled cell samples were treated with 30% hydrogen peroxide, 10% hydroxylamine, 0.5% ferrozine, and 500 μL of pyridine, following which the OD_{562} was measured with an ultraviolet-visible spectrophotometer (Shimadzu UV-1700, Columbia, MD), along with $FeCl_2$ standards.

Microscopic Analysis of Particle Uptake

SPIO-labeled cells were stained for the presence of internalized iron oxide particles using a Prussian blue stain (10). Using this method, the magnetic particles were converted to an intense dark blue color following 30 min of incubation with Perls' reagent (1 g of potassium ferrocyanide in 42 mL of deionized water + 8 mL of 37.5% HCl). SPIO uptake in washed and labeled 4% glutaraldehyde-fixed cells was visualized using a Zeiss Cell Observer System with ApoTome 2 digital imaging (Zeiss, Thornwood, NY). For TEM, washed and labeled cell samples were fixed with 3.0% formaldehyde, 1.5% glutaraldehyde in 0.1 M sodium cacodylate, 5 mM Ca^{2+}, and 2.5% sucrose. After staining with Palade's OsO_4 and uranyl acetate, cellular uptake in Epon-embedded cell samples was analyzed with an FEI Tecnai 12 TWIN TEM operating at 100 kV.

MPS Measurements

The signal response of counted numbers of SPIO-labeled cells was measured using MPS. For signal excitation, the samples were exposed to a homogeneous magnetic field oscillating at 25 kHz with an amplitude of 10 mT. The resulting signal was detected with a bandwidth of 2.5 MHz and was averaged over 30 s. The detected spectrum consists of odd harmonics of the excitation frequency that are produced by the magnetic nanoparticles. The amplitudes of low harmonics are proportional to the amount of particles and their signal yield, whereas high harmonics indicate the spatial resolution that can be achieved. To test the linearity of the signal in a concentration series, it therefore suffices to extract the respective amplitude of the third harmonic converted to units of Am^2.

Cell Transplantation

Animal experiments were performed in accordance with protocols approved by our Institutional Animal Care and Use Committee. UW particle-labeled MSCs were bilaterally transplanted in the striatum of 8-week-old male FvBn mice as described previously (11). Briefly, under 1.5% isoflurane anesthesia, mice

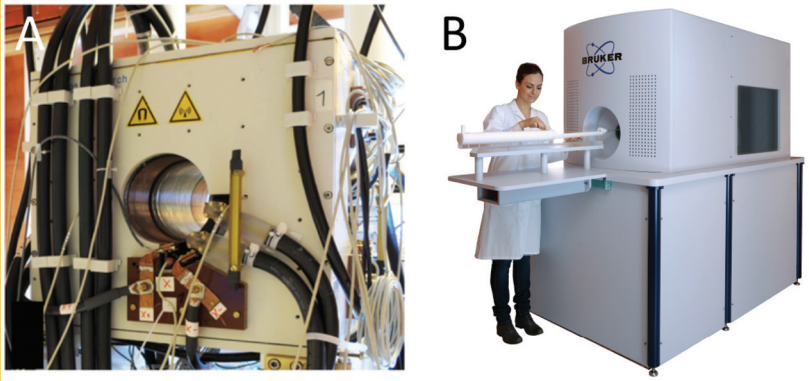

Figure 1. (A) Preclinical MPI scanner with a 12-cm bore used in this study. Selection field strength is 1.25 T/m in the *x* and *y* directions and 2.5 T/m in the *z* direction. The scanner uses 3 sets of drive field coils to enable 3D imaging. The Lissajous trajectory has a repetition time of 21.5 s, corresponding to encoding 46.4 volumes per second. 2D imaging in the *x*-*y* plane covers a maximum volume of approximately 25 × 25 × 1 mm^3. Additional focus field coils allow the volume to be moved out of the isocenter. A currently available commercial MPI scanner is shown in (B).

(n = 2) were positioned in a stereotaxic device (Stoelting, Woodsdale, IL). A small skin incision was made in the midline to expose the skull. Different cell densities (2×10^3, 1×10^4, 5×10^4, or 1×10^5 cells in 2 μL of phosphate-buffered saline) were injected using a pico-injector (Harvard Apparatus, Holliston, MA) with an attached pulled glass pipette (70-μm tip). Cells were injected slowly over 4 min, and the needle was left in place for 1 min before being withdrawn. One hour after transplantation, mice were euthanized and perfused with 4% paraformaldehyde, and the brains were removed. After postfixation for 2 days in 4% paraformaldehyde, samples were transferred to Fomblin (a polyperfluoroether devoid of a proton signal).

MRI Experiments

Imaging was performed on a vertical-bore 17.6-T nuclear magnetic resonance spectrometer (Bruker Biospin, Billerica, MA) equipped with a micro 2.5 gradient system. A 25-mm diameter volume coil was used for radiofrequency transmission and reception. Sagittal images were acquired using a T_2^* multigradient echo with a retention time of 500 ms, echo time between 5 and 50 ms, number of averages = 1, 256 × 196 × 196 matrix, and 16 × 13 × 13-mm field of view (66-μm isotropic resolution).

MPI Experiments

MPI experiments were conducted using a preclinical prototype scanner system (Figure 1). The scanner was operated in a 2D mode, where 2D slices were acquired in the horizontal (*x*-*y*) plane. In MPI, a static selection field gradient is required for spatial encoding, and its magnitude is directly related to the achievable spatial resolution. The MPI scanner was operated with a selection field gradient of 2.50 T/m in a vertical (*z*) direction and 1.25 T/m along the bore (*x*) and in the lateral direction (*y*). Drive fields were applied for signal generation with amplitudes of 16 mT in the *x* and *y* directions and 1 mT in the *z* direction. Thus, a quasi-2D volume of 25.6 × 25.6 × 0.8 mm^3 was encoded by the field-free point. The encoding time per plane was 21 ms. For improving the signal-to-noise ratio, 64 repetitions were averaged, resulting in an imaging time per plane of 13.8 s. Homogenous focus fields were applied to shift slices in the vertical direction. For covering the brains, 18 slices were stacked with a center-to-center distance of 1 mm so that an encoded imaging volume of 25.6 × 25.6 × 17.8 mm^3 resulted.

For image reconstruction in MPI, a system function was acquired that established the relation between spatial particle position and signal response. To this end, a small calibration sample consisting of particles deposited in a gel was moved stepwise by a robot to the 41 × 41 × 8 positions of a 3D grid with an isotropic interposition distance of 1.0 mm. The spatial extent of the calibration sample was between 3 and 6 mm, thus limiting the spatial resolution that could be reconstructed. Using the acquired system function, the 18 measured quasi-2D slices were reconstructed individually. For MPI of 50-μL volumes of pelleted cells, a grid of 23 × 23 × 1 positions was used with a pixel size of 2 × 2 mm^3, whereas all other imaging parameters remained unchanged. To visualize all samples despite their vast differences in concentration, regularization in image reconstruction was adapted for each concentration to deliver a good balance between signal-to-noise ratio and spatial resolution.

RESULTS

MPS Studies: Particle Efficacy and Quantification of Intracellular Iron and Labeled Cells

Acid-digested labeled cell samples were assayed for iron content using a spectrophotometric assay and ferric-ion specific dye. The mean iron content per cell was determined to have a range between 1 and 15 pg of Fe per cell, as listed in Table 1. Labeled cell suspensions at various concentrations were then investigated for their superparamagnetic efficacy in changing the MPS

Table 1. Mean Intracellular Fe Content

	Resovist	Feridex	UW Particles
NSC (~10 μm diameter cell body)	1.97	0.84	9.0
MSC (~25 μm diameter cell body)	13.67	4.21	13.0

Values are expressed as picograms of Fe per cell.

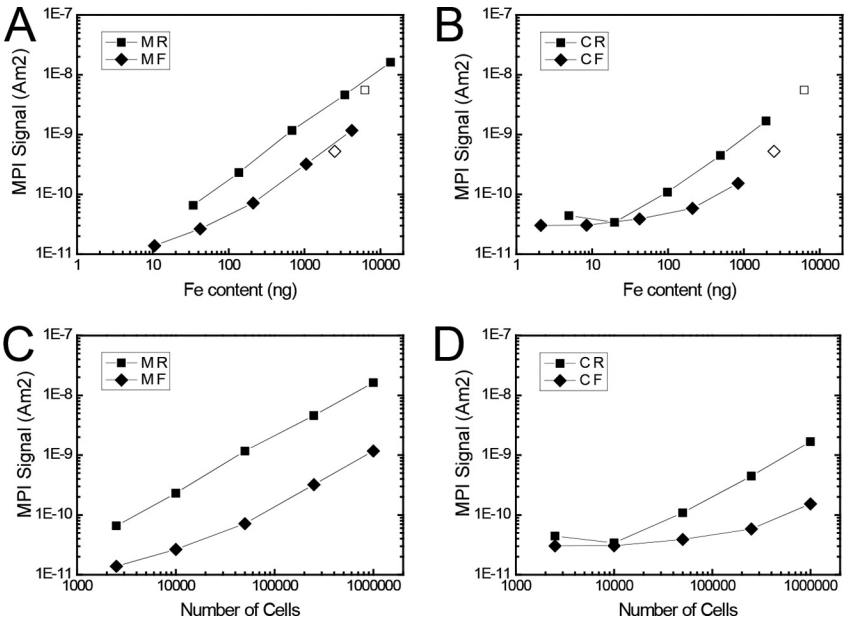

Figure 2. MPS signal measurements of MSCs and NSCs labeled with commercial, clinically used SPIO formulations. Shown are the MPI signal amplitudes as a function of Fe content (A and B) and the corresponding number of cells (C and D) obtained for the third harmonic. Data are shown for MSCs labeled with Resovist (MR) and Feridex (MF) and NSCs labeled with Resovist (CR) and Feridex (CF). Note the linearity of the MPS signal with both the iron content and number of cells except for the lowest concentration of the smaller NSCs (2500 cells) that contain less iron. Reference samples (free, noncell-bound particles in gelatin) are included in (A) and (B) as open symbols, with no difference in signal from cell-internalized particles.

signal. Figure 2 shows the MPS signal plots as a function of iron content (A and B) and corresponding cell number (C and D) for the 2 commercial SPIO preparations. Reference gelatin samples with free (noncell-bound SPIO particles are included for reference in A and B). Except for the lowest amount of the smaller NSCs, which had <1 pg of Fe per cell, there was a linear relation between the MPI signal and iron content. Slope values for the third harmonic were 1.2×10^{-3} Am^2/g Fe for MSCs + Resovist (R), which is equivalent to 1.7×10^{-14} Am^2 per cell; 2.8×10^{-4} Am^2/g Fe for MSCs + Feridex (F), or 1.2×10^{-15} Am^2 per cell; 8.6×10^{-4} Am^2/g Fe for NSCs + R; and 1.7×10^{-4} Am^2/g Fe for NSCs + F. Note that for both SPIO particle preparations, the SPIO-gelatin reference samples (without cells) have the same MPS value vs unit of iron as for the cell samples (Figure 2, A and B). For all samples, Resovist had a 4-fold higher MPI efficacy (on the third harmonic) per unit of iron compared with Feridex. This large difference was observed for both NSCs and MSCs. These values are summarized in Table 2.

For the experimental, preclinical UW SPIO formulation (Figure 3), the slope values for the third harmonic were 1.5×10^{-3} Am^2/g Fe for MSCs, which is equivalent to 2.0×10^{-14} Am^2 per cell; and 2.7×10^{-3} Am^2/g Fe for NSCs, amounting to 2.4×10^{-14} Am^2 per cell (Table 2). The SPIO-gelatin reference samples (without cells) again exhibited the same MPS value vs unit of iron as for the cell samples.

Table 2. MPS Signal Efficacy (Performance) Values

	Resovist	Feridex	UW Particles
NSC	8.6×10^{-4}	1.7×10^{-4}	2.7×10^{-3}
MSC	1.2×10^{-3}	2.8×10^{-4}	1.5×10^{-3}

Values are expressed as Am^2/g Fe.

Morphological Characterization of SPIO Labeling

The core size of the UW particles was calculated to be 19.0 nm using Chantrell fitting to the VSM magnetization curve. These results matched well with our TEM analysis (Figure 4A). From dynamic laser scattering measurements, the UW particles were calculated to have a hydrodynamic size of approximately 95 nm. Trypan blue viability staining showed >95% cell viability after labeling with all 3 SPIO tracers. Intracellular labeling was confirmed by Prussian blue staining (Figure 4B). The particles demonstrated a typical perinuclear focal accumulation. This is where the microtubuli end; the particles are transported along the microtubule filaments from the plasma membrane toward the cell interior. TEM demonstrated that the particles were bound to the cell membrane and were transported into intracellular vesicles (Figure 4C).

MPI Studies: Sensitivity and Quantification

Samples used for MPS measurements were further investigated for their detectability by MPI. UW-labeled NSCs in 50-μL gelatin samples demonstrated a detection threshold of about 3×10^4 cells (Figure 5). UW-labeled MSCs were then bilaterally transplanted into the mouse brain, after which both MRIs and MPIs were obtained (Figure 6). The lowest amounts of cells injected

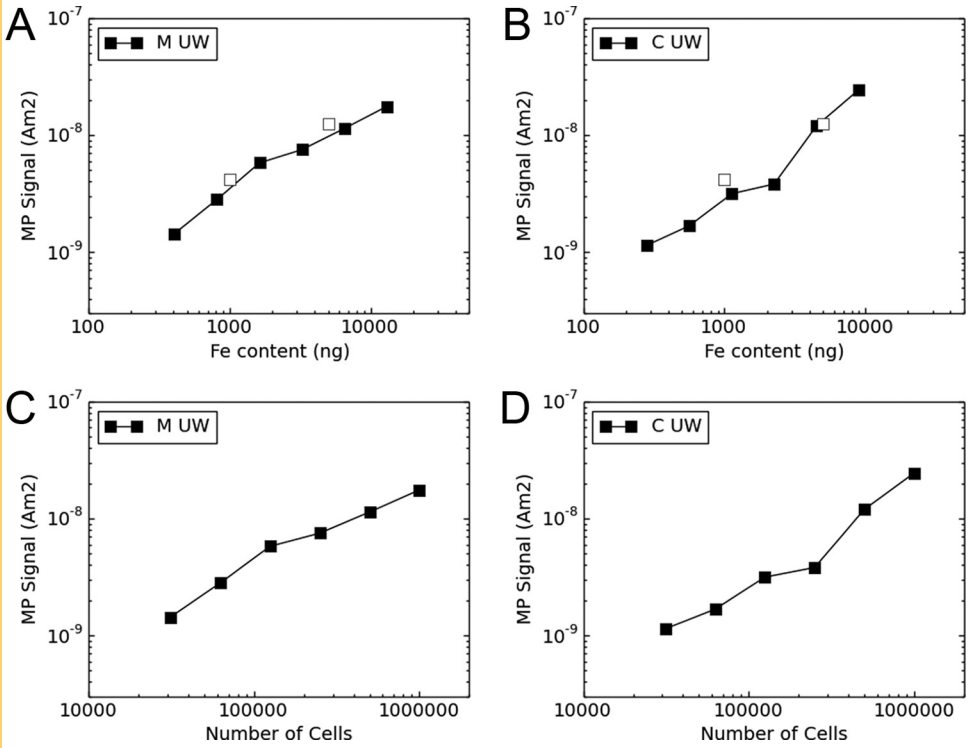

Figure 3. MPS signal measurements of MSCs and NSCs labeled with preclinical UW SPIO particles. Shown are the MPI signal amplitudes as a function of Fe content (A and B) and the corresponding number of cells (C and D) obtained for the third harmonic. Data are shown for MSCs (M UW) and NSCs (C UW). Note the linearity of the MPS signal with both the iron content and number of cells. Reference samples (free, noncell-bound particles in gelatin) are included in (A) and (B) as open symbols, with, again, no difference in signal from cell-internalized particles.

(2×10^3 and 1×10^4) could not be detected (data not shown). The threshold of detection was determined to be approximately 5×10^4 cells, which corresponds roughly to the number of cells that could be visualized in the gelatin phantoms (Figure 5). The overlay of the MPIs and MRIs showed a good anatomical correspondence of the areas of the striatum containing labeled cells. Quantification of the MPI signal revealed that the total signal obtained corresponded well to the number of cells injected (Figure 6D), with an amplitude ratio of 2.08 for 100 000 cells relative to 50 000 cells.

DISCUSSION

We have shown that SPIO-labeled stem cells can be detected with both MRI and MPI. The MPI signal was found to be linear with iron concentration and cell number, allowing for proper cell quantification. Importantly, as the conformational state of SPIO, which may range from intracellular clustering to free homogeneous particle suspensions, is often a priori not known, it avoids a major pitfall that exists with MRI quantification approaches, where the T_2/T_2^* relaxivity and contrast enhancement are not independent from the size of the SPIO clusters. Because the SPIO tracers are detected directly with MPI and not indirectly as in the case of MRI (where the signal is derived from protons), their quantification is simple and straightforward. This can be considered to be somewhat analogous to ^{19}F MRI, where the naturally abundant ^{19}F isotope is also detected directly (12). Fluorine MRI cell tracking has recently gained interest, with phase I clinical trials in progress (13, 14). It remains to be seen if

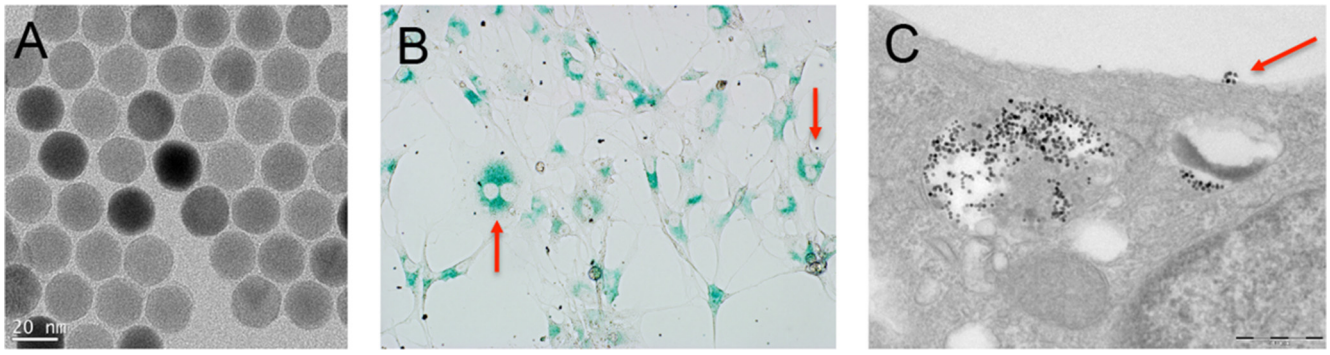

Figure 4. (A) TEM of UW particle preparation used for cell labeling. Note the near-perfect uniformity of shape and iron oxide core diameter (19 nm). (B) Prussian blue staining of UW-labeled MSCs. The SPIO particles are present as intracellular, perinuclear aggregates. Arrows indicate dividing cells (2 nuclei). (C) TEM of UW-labeled MSCs. After sticking to the cell membrane (arrow), the SPIO particles are internalized by macropinocytosis and are present in intracellular vesicles.

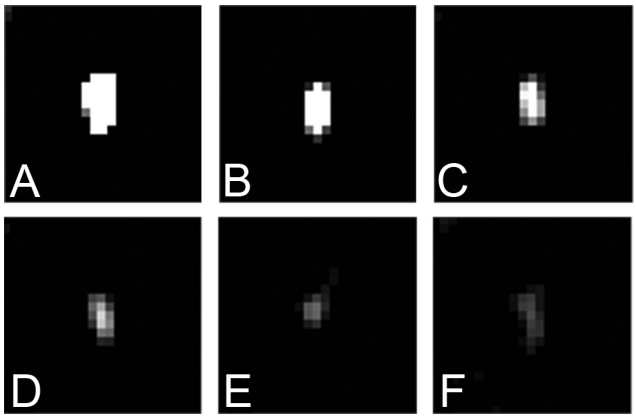

Figure 5. MPI of UW-labeled NSCs (50-μL gelatin samples) for (A) 1×10^6, (B) 5×10^5, (C) 2.5×10^5, (D) 1.25×10^5, (E) 6.25×10^4, and (F) 3.13×10^4 cells.

the sensitivity of MPI will exceed that of ^{19}F MRI, but in theory it should be possible to image cell numbers as low as 100 with dedicated instrumentation. Our current MPI detection threshold of 3-5 $\times$ 10^4 cells is similar to our preclinical ^{19}F MRI studies of fluorinated NSCs implanted in the mouse brain striatum, where we found a detection threshold of approximately 4×10^4 cells (15).

In the past, Feridex and Resovist have been most widely used for MRI cell tracking studies, including clinical trials (6). Unfortunately, because of economic reasons, these preparations are no longer commercially available. This prompted us to test alternative SPIO preparations and to further develop UW particles as an alternative MPI cell-tracking agent. We have tested several other SPIO preparations from other sources that have previously been successfully used in MRI; none exhibited sufficient MPI performance to be of further interest. We found that Resovist had a 4-fold higher MPI efficacy per unit of Fe than Feridex for the 2 differently sized stem cell types tested. This does not readily translate from the MRI contrast-enhancing properties; their MR relaxivities are about the same at a given field strength. This indicates that there is room for further optimization of MPI SPIO tracers, as their properties for optimal performance do not appear to automatically follow those for MRI. We found that the UW SPIO formulation slightly outperformed that of Resovist. To make the efficacy/performance of SPIO tracers comparable across different studies, we propose to introduce an "efficacy" or "performance" term with Am^2/g Fe as the unit (which had calculated values of 1×10^{-3} to 3×10^{-4} for the SPIO tracers in this study), ie, MPI signal per unit

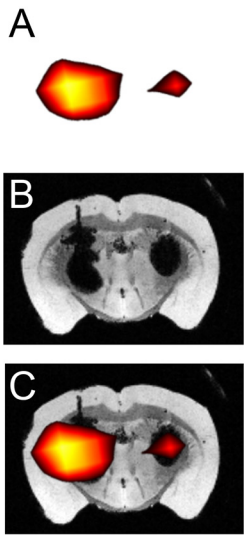

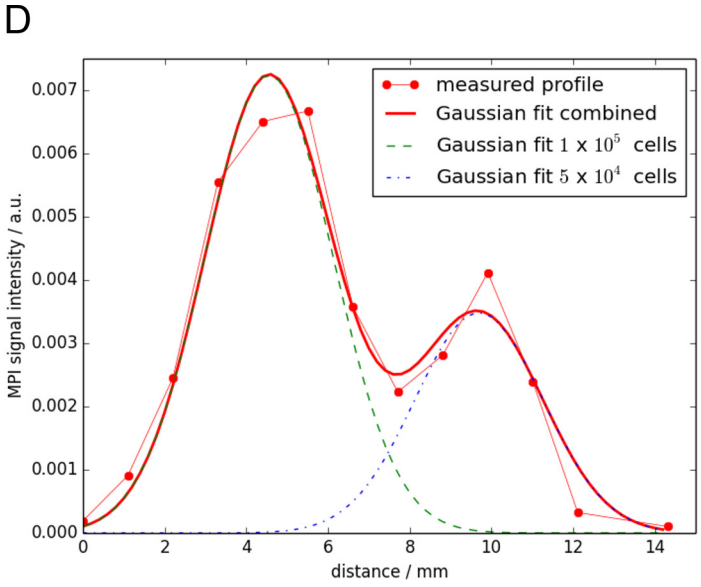

Figure 6. (A) MPI, (B) MRI, and (C) corresponding overlay MPI/MRI of a mouse brain transplanted with 1×10^5 (left hemisphere) or 5×10^4 (right hemisphere) UW-labeled MSCs. (D) Quantification of MPI signal measurements show an excellent correlation between the measured MPI signal and number of implanted cells. An intensity profile through the centers of both MPI signal peaks was extracted and fitted with 2 Gaussian curves. Five parameters were fitted, namely the amplitudes, positions, and 1 width parameter, which was assumed to be the same for both curves because it is mainly determined by the extent of the calibration sample used for system calibration. Fitted amplitude values were 7.24×10^{-3} and 3.48×10^{-3} arbitrary units at 4.55 and 9.69 mm for 1×10^5 and 5×10^4 cells, respectively, with a full width (resolution) of 3.68 mm.

concentration of SPIO, analogous to the term "MR relaxivity" used in MRI. This should then be specified for a specific MPI harmonic number, just as the applied specific magnetic field strength for MRI.

The development of MPI instrumentation is currently in full swing (16-19). We have learned a lot from cell tracking with MRI, and it is possible that MPI cell tracking can be readily adapted (20). However, a major drawback of hot-spot imaging techniques such as MPI is the lack of anatomical information. Other hot-spot imaging techniques, including single-photon emission computed tomography and positron emission tomography, are often combined with computed tomography or MRI. It remains to be seen whether MPI is best combined with computed tomography or MRI, but there are efforts to build a hybrid MPI/MRI system (21). There are no theoretical limits toward building a clinical MPI instrument (22, 23), and attempts to do so are already underway. However, and perhaps most importantly, the future of clinical MPI cell tracking will also depend on the availability of a clinically approved tracer formulation. In addition, expensive SPIO MPI tracer dose-toxicity studies will be needed to make the prospect of clinical MPI cell tracking a reality.

ACKNOWLEDGMENTS

We thank H. Boeve and J. Weizenecker for initial measurements and S.-H. Shin, D. Kadayakkara, and S. Bernard for experimental assistance. J. Borgert, D.E. Markov, J.C.J. Aerts, and M. Kuhn were critical in getting this project initiated. This work was supported by a grant from Philips Healthcare, Inc., the National Institutes of Health (EUREKA RO1 DA026299), and the German Federal Ministry of Education and Research (FKZ 13N9079, FKZ 13N11086).

Conflicts of Interest: K.M.K. is a founding partner in LodeSpin Labs, LLC, a Seattle-based biomedical start-up company. A.H., B.G., and J.R. are employees of Philips Healthcare.

REFERENCES

1. Cromer Berman SM, Walczak P, Bulte JW. Tracking stem cells using magnetic nanoparticles. Wiley Interdiscip Rev Nanomed Nanobiotechnol. 2011;3(4):343–355.
2. Ahrens ET, Flores R, Xu H, Morel PA. In vivo imaging platform for tracking immunotherapeutic cells. Nature Biotech. 2005;23(8):983–987.
3. Bulte JW. Hot spot MRI emerges from the background. Nat Biotechnol. 2005; 23(8):945–946.
4. Bulte JW, Gleich B, Weizenecker J, Bernard S, Walczak P, Borgert J, Aerts H, Boeve H. Developing cellular MPI: initial experience. Proc ISMRM. 2008;16: 1675.
5. Gleich B, Weizenecker J. Tomographic imaging using the nonlinear response of magnetic particles. Nature. 2005;435(7046):1214–1217.
6. Bulte JW. In vivo MRI cell tracking: clinical studies. AJR Am J Roentgenol. 2009; 193(2):314–325.
7. Hufschmid R, Arami H, Ferguson RM, Gonzales M, Teeman E, Brush LN, Browning ND, Krishnan KM. Synthesis of phase-pure and monodisperse iron oxide nanoparticles by thermal decomposition. Nanoscale. 2015;7(25):11142–11154.
8. Arami H, Khandhar AP, Tomitaka A, Yu E, Goodwill PW, Conolly SM, Krishnan KM. In vivo multimodal magnetic particle imaging (MPI) with tailored magneto/optical contrast agents. Biomaterials. 2015;52:251–261.
9. Soleimani M, Nadri S. A protocol for isolation and culture of mesenchymal stem cells from mouse bone marrow. Nat Protoc. 2009;4(1):102–106.
10. Bulte JW, Arbab AS, Douglas T, Frank JA. Preparation of magnetically labeled cells for cell tracking by magnetic resonance imaging. Methods Enzymol. 2004; 386:275–299.
11. Walczak P, Kedziorek DA, Gilad AA, Lin S, Bulte JW. Instant MR labeling of stem cells using magnetoelectroporation. Magn Reson Med. 2005;54(4):769–774.
12. Ruiz-Cabello J, Barnett BP, Bottomley PA, Bulte JW. Fluorine (19F) MRS and MRI in biomedicine. NMR Biomed. 2011;24(2):114–129.
13. Ahrens ET, Helfer BM, O'Hanlon CF, Schirda C. Clinical cell therapy imaging using a perfluorocarbon tracer and fluorine-19 MRI. Magn Reson Med. 2014; 72(6):1696–1701.
14. Rose LC, Kadayakkara DK, Wang G, Bar-Shir A, Helfer BM, O'Hanlon CF, et al. Fluorine-19 labeling of stromal vascular fraction cells for clinical imaging applications. Stem Cells Transl Med. 2015 Nov 18:pii:sctm.2015-0111.
15. Ruiz-Cabello J, Walczak P, Kedziorek DA, Chacko VP, Schmieder AH, Wickline SA, Lanza GM, Bulte JW. In vivo "hot spot" MR imaging of neural stem cells using fluorinated nanoparticles. Magn Reson Med. 2008;60(6):1506–1511.
16. Goodwill PW, Lu K, Zheng B, Conolly SM. An x-space magnetic particle imaging scanner. Rev Sci Instrum. 2012;83(3):033708.
17. Saritas EU, Goodwill PW, Croft LR, Konkle JJ, Lu K, Zheng B, Conolly SM. Magnetic particle imaging (MPI) for NMR and MRI researchers. J Magn Reson. 2013; 229:116–126.
18. Buzug TM. Magnetic particle imaging—from particle science to imaging technology. Biomed Tech (Berl). 2013;58(6):489–491.
19. Hong H, Lim J, Choi CJ, Shin SW, Krause HJ. Magnetic particle imaging with a planar frequency mixing magnetic detection scanner. Rev Sci Instrum. 2014; 85(1):013705.
20. Bulte JW, Walczak P, Gleich B, Weizenecker J, Markov DE, Aerts HC, Boeve H, Borgert J, Kuhn M. MPI cell tracking: what can we learn from MRI? Proc Soc Photo Opt Instrum Eng. 2011;7965:79650z.
21. Franke J, Heinen U, Lehr H, Weber A, Jaspard F, Ruhm W, Heidenreich M, Schulz V. First 3D dual modality phantom measurements of a hybrid MPI-MRI system using a resistive 12 channel MPI-MRI magnet design. International Workshop on Magnetic Particle Imaging (IWMPI). 2015;doi: 101109/IWMPI20157106990.
22. Weizenecker J, Gleich B, Rahmer J, Dahnke H, Borgert J. Three-dimensional real-time in vivo magnetic particle imaging. Phys Med Biol. 2009;54(5):L1–L10.
23. Borgert J, Schmidt JD, Schmale I, Bontus C, Gleich B, David B, Weizenecker J, Jockram J, Lauruschkat C, Mende O, Heinrich M, Halkola A, Bergmann J, Woywode O, Rahmer J. Perspectives on clinical magnetic particle imaging. Biomed Tech (Berl). 2013;58(6):551–556.